ChemComm

Check for updates

Noncovalent interaction network of chalcogen, halogen and hydrogen bonds for supramolecular β-sheet organization†

Jinlian Cao,‡[a] Peimin Weng,‡[b] Yuanwei Qi,[c] Kexin Lin[c] and Xiaosheng Yan ✶[c]

An alanine-based bilateral building block, linked by 2,5-thiophenediamide motifs and equipped with C-terminal 4-iodoaniline groups, was designed, allowing a noncovalent interaction network consisting of intramolecular chalcogen bonds and intermolecular halogen/hydrogen bonds, which cooperatively maintain a supramolecular β-sheet organization in the solid state, as well as in dilute CH_3CN solution with a high g factor of −0.017.

Intermolecular noncovalent interactions play critical roles in maintaining supramolecular assemblies with diverse structures and functions, wherein multiple noncovalent interactions can cooperate to promote both the formation and stabilization of the assemblies.[1,2] It is important to note that in biological systems, not only intermolecular interactions but also intramolecular interactions contribute to the stability and organization of assemblies. For instance, intra-helix hydrogen bonding in protein α-helices and π···π stacking between DNA base pairs are crucial for their structural integrity.[3,4] This realization has inspired the construction and regulation of supramolecular assemblies through the introduction of intramolecular interactions. A significant advancement in this aspect is building biomimetic supramolecular helices using helical building blocks.[5] In such systems, intramolecular interactions, such as hydrogen bonds and π···π stacking,[6–13] maintain the helical conformation of the building blocks and pre-organize the intermolecular interaction sites in optimal positions, promoting the tendency and stability

of helical assemblies. Upon helix formation, intramolecular interactions could be enhanced to maintain the molecular helical conformation.

In this context, we have developed short peptide-based *N*-amidothioureas, wherein an intramolecular ten-membered ring hydrogen bond can maintain a helical β-turn conformation,[14–16] which facilitates intermolecular halogen bonds to allow the formation of single and double supramolecular helices in both the solid state and solution phase.[17–19] Intriguingly, the incorporation of a 2,5-thiophenediamide linker into bilateral *N*-amidothiourea building blocks would afford intramolecular chalcogen bonds, allowing a noncovalent interaction network consisting of intramolecular hydrogen/chalcogen bonds and intermolecular halogen bonds, which leads to a supramolecular helix of stronger supramolecular helicity and higher thermal stability.[20] This highlights the cooperative nature of intra- and intermolecular interactions in supporting helical assemblies.

Besides helical structures, β-sheets are another essential biological structure that plays a crucial role in maintaining the conformation and functionality of proteins.[21] The development of artificial biomimetic supramolecular β-sheet structures from self-assembling peptides or amino acids is an exciting and promising field with potential applications in materials science and bioengineering.[22–24] However, the cooperative effects of intra- and intermolecular interactions in maintaining supramolecular β-sheet structures have yet to be demonstrated, as traditional β-sheet organizations are primarily only supported by intermolecular interactions, *e.g.* hydrogen bonds.

Herein, we propose to regulate the supramolecular β-sheet organization using intramolecular interactions, achieved by forming a network of intra- and intermolecular noncovalent interactions that work together in a cooperative manner. For this purpose, we designed alanine-based bilateral building block **1** (Scheme 1), which features a 2,5-thiophenediamide linker and 4-iodoaniline groups at both ends. The alanine-based amide bonds can afford intermolecular hydrogen bonds in a β-sheet manner, in considering that unfolded short peptides tend to adopt a β-sheet organization.[25,26] Moreover, the

[a] *The Higher Educational Key Laboratory for Flexible Manufacturing Equipment Integration of Fujian Province, Xiamen Institute of Technology, Xiamen 361021, China*
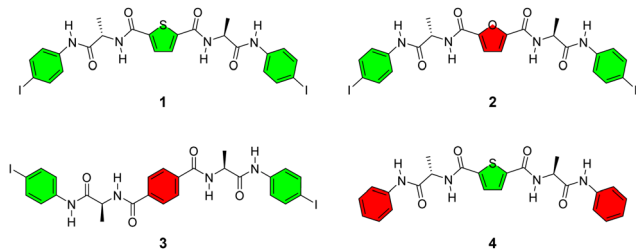
[b] *Peking University Yangtze Delta Institute of Optoelectronics, 226010, Nantong, Jiangsu, China*

[c] *Fujian Provincial Key Laboratory of Innovative Drug Target Research and State Key Laboratory of Cellular Stress Biology, School of Pharmaceutical Sciences, Xiamen University, Xiamen, Fujian, 361102, China. E-mail: xshyan@xmu.edu.cn*

Scheme 1 Molecular structures of alanine-based bilateral building blocks **1**, **2**, **3** and **4**. Compound **1** features a 2,5-thiophenediamide linker and C-terminal 4-iodoaniline groups. Control compounds **2** with a 2,5-furandiamide linker, **3** with a terephthalamide linker, and **4** without terminal iodine atoms are designed to illustrate the importance of the intramolecular chalcogen bonds and intermolecular halogen bonds for the assembly of **1**. All alanine residues are of ʟ-configuration.

2,5-thiophenediamide motif is known to form intramolecular chalcogen bonds,[20] and the terminal iodine atoms can participate in intermolecular halogen bonding.[27] These noncovalent interactions facilitate the assembly of the building block **1** by creating an interaction network. Our experiments have confirmed the formation of a biomimetic supramolecular β-sheet structure in both the solid state and dilute CH_3CN solution, supported by a noncovalent interaction network consisting of intramolecular chalcogen bonds and intermolecular halogen/hydrogen bonds. The g factor of the assembled structure measures up to −0.017, together with a twisted tape morphology. To further understand the role of specific interactions, we designed control compounds **2**, **3** and **4** (Scheme 1), which feature variations in the linker and the absence of terminal iodine atoms. By comparing the structures of the control compounds with that of **1**, the significance of intramolecular chalcogen bonds and intermolecular halogen bonds in organizing the β-sheet structure can be illustrated.

Alanine-based bilateral building blocks **1**–**4** were synthesized following the procedures outlined in Schemes S1–S4 (ESI†). Initially, we measured the absorption and CD spectra of **1**–**4** in solution. Comparison with **2**, **3** and **4** revealed distinct features of **1**. Specifically, in dilute CH_3CN solution, **1** displayed a red-shifted CD spectrum with significantly stronger Cotton effects at 304 nm and 250 nm. Concomitantly, the absorption spectrum exhibited reduced absorbance and an increased baseline (Fig. 1a). These observations suggest the possible formation of supramolecular chiral assemblies from **1** in CH_3CN solution.

The g factor profiles, derived from the absorption and CD spectra (Fig. S1, ESI†),[28] disclosed a remarkably high g factor for **1** in CH_3CN, particularly at 307 nm, where it reached −0.017 (Fig. 1b). This value is 6, 27 and 34 times higher than that of **2**, **3** and **4**, respectively. The CD spectra of **1** in CH_3CN further demonstrated its pronounced sensitivity to changes of solution temperature, exhibiting a substantial decrease in CD signals upon heating (Fig. S2, ESI†). This observation further supports the hypothesis of supramolecular polymeric species formation from **1** in CH_3CN.

Dynamic light scattering (DLS) was next employed, revealing the presence of polymeric species of **1** with diameters approximately
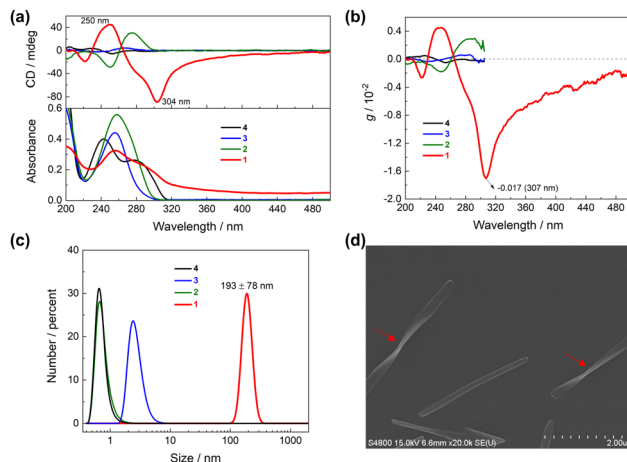
Fig. 1 (a) Absorption and CD spectra of **1**, **2**, **3** and **4** in CH_3CN. (b) The g factor profiles of **1**, **2**, **3** and **4**. For clarity, the fluctuated profiles of **2**, **3** and **4** at long wavelengths (>305 nm) are omitted (Fig. S1, ESI†). (c) Hydrodynamic diameters of **1**, **2**, **3** and **4** in CH_3CN measured by dynamic light scattering. (d) SEM image of the air-dried sample from CH_3CN solution of **1** on a platinum coated silicon wafer. [**1**] = [**2**] = [**3**] = [**4**] = 10 μM.

193 nm, while monomers were observed for **2**, **3** and **4** in CH_3CN (Fig. 1c). SEM images of solution samples of **1** exhibited an ordered tape morphology (Fig. S3, ESI†), characterized by lengths and widths centred at 1.75 μm and 0.22 μm, respectively (Fig. S4, ESI†). Notably, most of the tape structures displayed a twist, specifically right-handed (Fig. 1d and S3, ESI†), indicating the supramolecular helicity of the polymeric species that contributes to the high g factor. Conversely, the SEM images of control compounds **2**, **3** and **4** exhibited amorphous blocks (Fig. S5, ESI†).

To gain insight into the structure and formation mechanism of polymeric species of **1** in CH_3CN, the molecular conformation and organization were investigated. Two potential conformations have been proposed for alanine-based building block **1** (Fig. 2a).[20] In conformation I, the 2,5-thiophenediamide linker enables two intramolecular C–S···O=C chalcogen bonds,
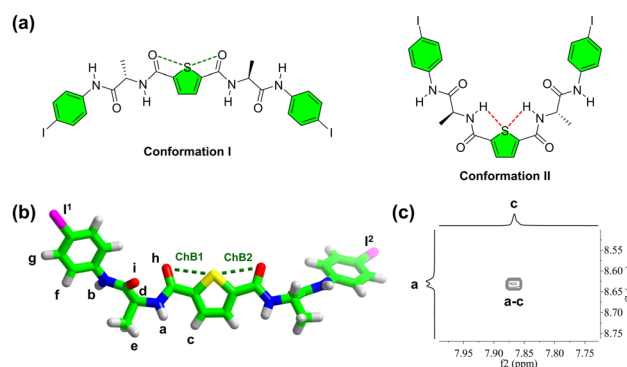
Fig. 2 (a) Two possible conformations of **1**, containing two intramolecular chalcogen bonds (I) and hydrogen bonds (II), respectively. (b) X-ray crystal structure of **1**, featuring two intramolecular C–S···ʰO=C chalcogen bonds (ChB1 and ChB2). (c) Partial 2D NOESY spectrum of **1** in 60:40 (v/v) CD_3CN/DMSO-d_6 mixtures. [**1**] = 2 mM.

while in conformation II, two intramolecular N–H···S–C hydrogen bonds are formed. To determine the conformation of **1**, both single crystal structure analysis and 1D/2D NMR were conducted. Crystals suitable for X-ray crystallography were obtained by slowly evaporating a DMF solution of **1**. Crystallographic data revealed that molecule **1** crystallized in the triclinic *P*1 space group, with one molecule in the asymmetric unit (Fig. S6 and Table S1, ESI†). In the crystal, compound **1** adopts *cis*-form with two intramolecular C–S···^{h}O=C chalcogen bonds (ChB1 and ChB2) afforded by the 2,5-thiophenediamide linker (Fig. 2b). The distances between S and ^{h}O atoms, measured as 3.061 Å (ChB1) and 3.028 Å (ChB2), respectively, are shorter than the sum of the van der Waals radii of O and S atoms (3.320 Å, details on the parameters of noncovalent interactions can be found in Table S2, ESI†). This structure is consistent with the proposed conformation I (Fig. 2a).

The 2D NOESY spectrum of **1**, acquired in 60:40 (v/v) CD$_3$CN/DMSO-d_6, revealed obvious coupling between the –NH^a and –CH^c protons (Fig. 2c and Fig. S7, ESI†), indicating the adoption of conformation I of **1** in the solution phase. Temperature-dependent ^{1}H NMR spectra of **1** demonstrated significant changes in the chemical shifts of –NH^a and –NH^b (−7.21 and −6.51 ppb °C in temperature coefficient, respectively, Fig. S8 and S9, ESI†). These observations suggest that –NH^a and –NH^b are not involved in intramolecular hydrogen bonding,[29] excluding the existence of conformation II of **1** in the solution phase. Consequently, **1** retains conformation I, characterized by two intramolecular C–S···^{h}O=C chalcogen bonds, both in the solid state and in the solution phase.

The molecular organization of **1** was then investigated by analysing its crystal structure. Along the *c*-axis of the crystal lattice, the molecules of **1** interact with each other *via* intermolecular C–I^1···^{2}I–C halogen bonds (XB1, Table S2, ESI†), effectively forming a chain. Additionally, along the *a*-axis, these chains align and stack through intermolecular N–H^b···^{i}O=C hydrogen bonds (HB1 and HB2, Table S2, ESI†). As a result, a halogen- and hydrogen-bonded two-dimensional (2D) structure forms within the *ac* plane of crystal **1** (Fig. 3a). This 2D structure bears resemblance to the parallel β-sheet structure found in biological systems (Table S3, ESI†),[21] where the C–I^1···^{2}I–C halogen bonds and N–H^b···^{i}O=C hydrogen bonds serve as intra- and inter-strand interactions, respectively. Furthermore, intramolecular chalcogen bonds (ChB1 and ChB2) contribute to a noncovalent interaction network involving chalcogen/halogen/hydrogen bonds (Fig. S10, ESI†), promoting the stabilization of the biomimetic β-sheet structure.

The 2D biomimetic supramolecular β-sheet structures within the *ac* plane of crystal **1** further stack in a parallel arrangement along the *b*-axis, facilitated by intermolecular N–H^a···^{h}O=C hydrogen bonds (HB3 and HB4) and C–I^2···^{1}I–C halogen bonds (XB2, Table S2, ESI†), leading to the formation of a three-dimensional (3D) structure (Fig. S11, ESI†). Within the *bc* plane, halogen bonds (XB1 and XB2) and hydrogen bonds (HB3 and HB4) support a 2D structure that also resembles a β-sheet (Fig. 3b), wherein two halogen bonds propagate along the *b*-axis alternately, utilizing an iodine atom as both the
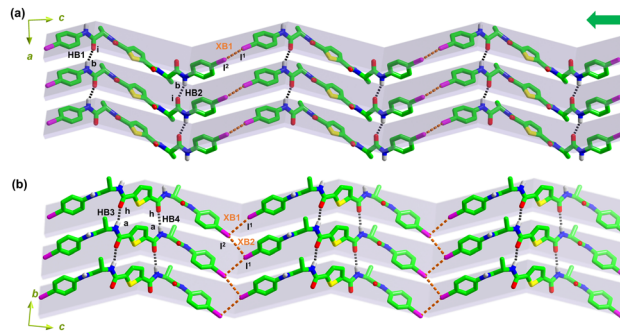

Fig. 3 (a) Supramolecular β-sheet structure within the *ac* plane of crystal **1**, supported by intermolecular XB1, HB1 and HB2 interactions. (b) Supramolecular β-sheet structure within the *bc* plane of crystal **1**, supported by intermolecular XB1, XB2, HB3 and HB4 interactions. For clarity, −CH protons are omitted. Dashed orange lines indicate intermolecular halogen bonds (XB1 and XB2), dashed black lines highlight intermolecular hydrogen bonds (HB1, HB2, HB3 and HB4). The green arrow indicates the direction of donor to acceptor halogen bonding along the biomimetic strand structure (*c*-axis).

donor and acceptor (Fig. S12, ESI†). Along the crystallographic *a*- and *b*-axes, the centroid–centroid distances of the aromatic rings are measured to be as long as 4.711 Å and 5.189 Å, respectively (Fig. S13, ESI†), suggesting that the contribution of π-stacking to the assembly is negligible.[30]

Therefore, in the 3D crystal structure, each **1** molecule participates in the formation of two intramolecular C–S···O=C chalcogen bonds (ChB1 and ChB2), four C–I···I–C halogen bonds (XB1 and XB2 doubled), and eight N–H···O=C hydrogen bonds (HB1, HB2, HB3, and HB4 doubled, Fig. 4a). These interactions together create a strong and resilient noncovalent interaction network that supports the biomimetic β-sheet organization of **1**. The Fourier transform infrared spectroscopy (FTIR) of **1** exhibited absorption peaks of the amide I region at 1676 and 1640 cm^{-1} (Fig. S14, ESI†), indicating the presence of the supramolecular β-sheet structure,[31,32] in line with the 3D crystal structure.

Notably, the CD spectrum of **1** in CH$_3$CN solution closely resembles that of the solid state (Fig. 4b), suggesting that **1** adopts a similar assembled structure, *i.e.* chalcogen, halogen and hydrogen-bonded biomimetic β-sheet organization, in the CH$_3$CN solution and the solid state. The absorption, CD and DLS profiles (Fig. S15, ESI†) indicate that the addition of polar DMSO to the CH$_3$CN solution causes a transition into the monomeric form of **1**, which can be attributed to the
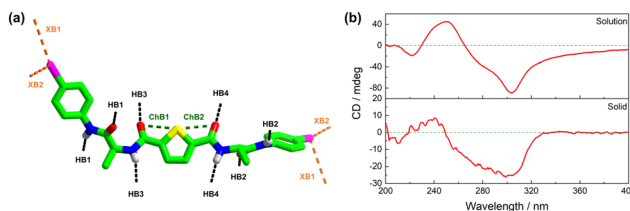

Fig. 4 (a) Noncovalent interaction network for each **1** molecule in the 3D crystal structure (dashed green lines, chalcogen bonds; dashed orange lines, halogen bonds; dashed black lines, hydrogen bonds). (b) CD spectra of **1** in CH$_3$CN solution and in the solid state.

competition between DMSO and intermolecular halogen and hydrogen bonds.

SEM images of **1** (Fig. 1d and Fig. S3, ESI†) reveal the existence of right-handed twisted tape morphology, which is accountable for the high *g* factor of **1** in the CH$_3$CN solution. This distinct feature bears a striking resemblance to naturally occurring β-sheets, where β-strands commonly exhibit a right-handed twist.[33,34] The crystal structure of **1** reveals that well-oriented hydrogen bonds propagate along the *a*- and *b*-axes, while along the *c*-axis only misaligned halogen bonds drive packing (Fig. 3), which may limit the lateral growth of the supramolecular tapes.

In the case of control compounds **2** and **3**, which have a 2,5-furandiamide linker and a terephthalamide linker, respectively, the absence of intramolecular chalcogen bonds prevents the formation of a strong noncovalent interaction network. As a result, **2** and **3** exist in a monomeric form in CH$_3$CN solution (Fig. 1). Control compound **4**, which lacks terminal iodine atoms, also adopts a monomeric form in CH$_3$CN due to the absence of intermolecular halogen bonds (Fig. 1). These observations highlight the cooperative nature of chalcogen, halogen and hydrogen bonds in the noncovalent interaction network of **1**, which facilitates the formation of the biomimetic β-sheet organization in both the solid state and dilute CH$_3$CN solution.

In summary, we proposed to introduce intramolecular interactions to regulate the formation of a supramolecular β-sheet structure, achieved by forming an intra- and intermolecular noncovalent interaction network. To this end, we designed an alanine-based bilateral building block, linked by a 2,5-thiophene-diamide motif and equipped with C-terminal 4-iodoaniline groups. This design allows for the establishment of a noncovalent interaction network that includes intramolecular chalcogen bonds and intermolecular halogen/hydrogen bonds. These interactions work cooperatively to maintain the supramolecular β-sheet structure, not only in the solid state but also in dilute CH$_3$CN solution, resulting in a high supramolecular chirality characterized by a *g* factor up to −0.017, as well as a twisted tape morphology. The control compounds lacking either intramolecular chalcogen bonds or intermolecular halogen bonds exhibit a loss of assembly behaviour in the CH$_3$CN solution, which emphasizes the importance of the cooperative noncovalent interaction network for the organization of the β-sheet structure. The significance of our findings lies in the potential to aid in the construction and regulation of supramolecular assemblies by incorporating both intra- and intermolecular interactions that can establish a robust noncovalent interaction network to support the assemblies. Ongoing efforts are being made to assess the performance in terms of recognition and transmembrane transport of the assemblies that are supported by synergistic intra- and intermolecular supramolecular interactions.

Conflicts of interest

There are no conflicts to declare.

Notes and references

1 A. S. Mahadevi and G. N. Sastry, *Chem. Rev.*, 2016, **116**, 2775–2825.
2 C. A. Hunter and H. L. Anderson, *Angew. Chem., Int. Ed.*, 2009, **48**, 7488–7499.
3 L. Pauling, R. B. Corey and H. R. Branson, *Proc. Natl. Acad. Sci. U. S. A.*, 1951, **37**, 205–211.
4 J. D. Watson and F. H. C. Crick, *Nature*, 1953, **171**, 737–738.
5 X. Yan, P. Weng, D. Shi and Y.-B. Jiang, *Chem. Commun.*, 2021, **57**, 12562–12574.
6 S. Mondal, L. Adler-Abramovich, A. Lampel, Y. Bram, S. Lipstman and E. Gazit, *Nat. Commun.*, 2015, **6**, 8615.
7 C.-Z. Liu, S. Koppireddi, H. Wang, D.-W. Zhang and Z.-T. Li, *Angew. Chem., Int. Ed.*, 2019, **58**, 226–230.
8 R. Misra, A. Saseendran, S. Dey and H. N. Gopi, *Angew. Chem., Int. Ed.*, 2019, **58**, 2251–2255.
9 S. Dey, R. Misra, A. Saseendran, S. Pahan and H. N. Gopi, *Angew. Chem., Int. Ed.*, 2021, **60**, 9863–9868.
10 D. Zhao and J. S. Moore, *J. Am. Chem. Soc.*, 2002, **124**, 9996–9997.
11 H. Zhao, W. Q. Ong, F. Zhou, X. Fang, X. Chen, S. F. Y. Li, H. Su, N.-J. Cho and H. Zeng, *Chem. Sci.*, 2012, **3**, 2042–2046.
12 S. Qi, C. Zhang, H. Yu, J. Zhang, T. Yan, Z. Lin, B. Yang and Z. Dong, *J. Am. Chem. Soc.*, 2021, **143**, 3284–3288.
13 D. Bai, T. Yan, S. Wang, Y. Wang, J. Fu, X. Fang, J. Zhu and J. Liu, *Angew. Chem., Int. Ed.*, 2020, **59**, 13602–13607.
14 X.-S. Yan, K. Wu, Y. Yuan, Y. Zhan, J.-H. Wang, Z. Li and Y.-B. Jiang, *Chem. Commun.*, 2013, **49**, 8943–8945.
15 X.-S. Yan, H. Luo, K.-S. Zou, J.-L. Cao, Z. Li and Y.-B. Jiang, *ACS Omega*, 2018, **3**, 4786–4790.
16 Y. Zhang, X. Yan, J. Cao, P. Weng, D. Miao, Z. Li and Y.-B. Jiang, *J. Org. Chem.*, 2020, **85**, 9844–9849.
17 J. Cao, X. Yan, W. He, X. Li, Z. Li, Y. Mo, M. Liu and Y.-B. Jiang, *J. Am. Chem. Soc.*, 2017, **139**, 6605–6610.
18 X. Yan, J. Cao, Y. Zhang, P. Weng, D. Miao, Z. Zhao, Z. Li and Y.-B. Jiang, *Chem. Commun.*, 2021, **57**, 1802–1805.
19 X. Yan, K. Zou, J. Cao, X. Li, Z. Zhao, Z. Li, A. Wu, W. Liang, Y. Mo and Y. Jiang, *Nat. Commun.*, 2019, **10**, 3610.
20 P. Weng, X. Yan, J. Cao, Z. Li and Y.-B. Jiang, *Chem. Commun.*, 2022, **58**, 6461–6464.
21 L. Pauling and R. B. Corey, *Proc. Natl. Acad. Sci. U. S. A.*, 1951, **37**, 729–740.
22 S. Kim, J. H. Kim, J. S. Lee and C. B. Park, *Small*, 2015, **11**, 3623–3640.
23 S. Bera, S. Mondal, S. Rencus-Lazar and E. Gazit, *Acc. Chem. Res.*, 2018, **51**, 2187–2197.
24 Y. Zhang, Q. Li, H. Wu, Y. Wang, Y. Wang, S. Rencus-Lazar, Y. Zhao, J. Wang, D. Mei, H. Xu, E. Gazit and K. Tao, *ACS Nano*, 2023, **17**, 2737–2744.
25 Z. Luo and S. Zhang, *Chem. Soc. Rev.*, 2012, **41**, 4736–4754.
26 W. J. M. FrederixPim, G. G. Scott, Y. M. Abul-Haija, D. Kalafatovic, C. G. Pappas, N. Javid, N. T. Hunt, R. V. Ulijn and T. Tuttle, *Nat. Chem.*, 2015, **7**, 30–37.
27 G. Cavallo, P. Metrangolo, R. Milani, T. Pilati, A. Priimagi, G. Resnati and G. Terraneo, *Chem. Rev.*, 2016, **116**, 2478–2601.
28 X. Cheng, T. Miao, L. Yin, Y. Ji, Y. Li, Z. Zhang, W. Zhang and X. Zhu, *Angew. Chem., Int. Ed.*, 2020, **59**, 9669–9677.
29 H.-J. Lee, K.-B. Lee, I.-A. Ahn, S. Ro, K.-H. Choi and Y.-S. Choi, *J. Pept. Res.*, 2000, **56**, 35–46.
30 A. Banerjee, A. Saha and B. K. Saha, *Cryst. Growth Des.*, 2019, **19**, 2245–2252.
31 V. Cabiaux, R. Brasseur, R. Wattiez, P. Falmagne, J. M. Ruysschaert and E. Goormaghtigh, *J. Biol. Chem.*, 1989, **264**, 4928–4938.
32 J. Seo, W. Hoffmann, S. Warnke, X. Huang, S. Gewinner, W. Schöllkopf, M. T. Bowers, G. von Helden and K. Pagel, *Nat. Chem.*, 2017, **9**, 39–44.
33 K. Fujiwara, S. Ebisawa, Y. Watanabe, H. Toda and M. Ikeguchi, *Proteins: Struct., Funct., Bioinf.*, 2014, **82**, 1484–1493.
34 K. Fujiwara, S. Ebisawa, Y. Watanabe, H. Fujiwara and M. Ikeguchi, *BMC Struct. Biol.*, 2015, **15**, 21.